Dynamics of gelatin ablation due to free-electron-laser irradiation

Jerri Tribble, Don C. Lamb,* Lou Reinisch, and Glenn Edwards
Department of Physics and Astronomy and Department of Otolaryngology, Vanderbilt University, Nashville, Tennessee 37235
(Received 7 January 1997)

We have carried out simultaneous, time-dependent measurements of the free-electron-laser (FEL)-induced stress transients and ablation plume in gelatin, which serves as a model system for collagenous tissues. The Mark-III FEL is tunable in the mid-IR (2–10 μm) and produces macropulses of microsecond duration comprised of picosecond micropulses separated by 350 ps. The macropulse duration was shortened with a broadband, IR Pockels cell, producing pulse durations as short as 60 ns and energies in the range of 0.1–1 mJ. The IR beam was focused to a diameter of 112–210 μm, depending on the wavelength, and measurements were made at 3.0, 3.36, and 6.45 μm. For fluences below the ablation threshold, stress transients were measured and accounted for with a standard thermoelastic mechanism. Of particular interest were the measurements with fluences above the ablation threshold, where two classes of dynamics were observed. A cw HeNe beam monitors the plume: at 3.0 μm a single maximum of the ''shadow'' is observed, while at 3.36 μm and 6.45 μm a second maximum also was resolved at later times. In addition, at 3.36 μm and 6.45 μm the duration of the momentum recoil is about twice as long as that observed for comparable exposure parameters at 3.0 μm. [S1063-651X(97)00606-5]

PACS number(s): 87.45.Bp

I. INTRODUCTION

Recently the advantage of ablating tissue with a free-electron laser (FEL) tuned near 6.45 μm was demonstrated [1]. More specifically, collateral damage was reduced and ablation rates were substantial for neural, ophthalmic, and dermal tissues. To account for these observations, a *thermodynamic* model for corneal stroma was proposed, where the photon energy is absorbed by the overlapping amide II mode of protein at 6.45 μm and the bending mode of water at 6.1 μm. It was proposed that the energy absorbed by protein compromises the structural integrity of the tissue while that absorbed by water results in vaporization and the explosive force. The essential quantitative feature of this model is the ratio of the enthalpy of the collagen-gelatin transition (55 J/g) to the latent heat of vaporization (2260 J/g). These results suggest that the *dynamics* of tissue ablation are not completely understood and may indeed be quite interesting. The importance of the FEL pulse structure for effective tissue ablation with infrared radiation has yet to be completely resolved.

Here we report on our investigation of the dynamics of infrared tissue ablation. The onset of the ablation plume was measured with a cw HeNe beam aligned parallel to the surface of gelatin, while a piezoelectric detector simultaneously monitored the acoustic transients. Gelatin serves as a model system for collagenous tissue.

II. EXPERIMENTAL METHOD

The Mark-III FEL is tunable from 2 to 10 μm and has both high peak and high average power due to a relatively complex pulse structure [2]. The spectral resolution is less than 0.03 μm (full width at half maximum). The Vanderbilt FEL currently produces a macropulse approximately 4 μs in duration with a repetition rate of up to 30 Hz. Each macropulse is comprised of approximately 10 000 micropulses of picosecond duration where the micropulse spacing is 350 ps. Micropulse energies are in the 10 μJ range and macropulse energies of up to 100 mJ are produced.

The experimental design is shown schematically in Fig. 1. FEL harmonics were essentially eliminated with either silicon or germanium filters, depending on the wavelength. Infrared Pockels cell technology was used to produce ''macropulses'' with durations ranging from 60 ns to 2 μs. At longer wavelengths a broadband Pockels cell with a Brewster cut CdTe crystal was used, with a typical extinction ratio of 1:200 [3]; however, the performance degraded near 3 μm, apparently due to a multiphoton process. Consequently, for 3.0 and 3.36 μm a normal-incidence Pockels cell was used where the size of the CdTe crystal was increased from 3 mm to >4 mm and the electronic logic was reversed relative to the broadband Pockels cell.

The IR beam was focused onto a gelatin sample under ambient conditions. The energy delivered to the sample was varied by crossed polarizers. A Molectron J25 detector measured the energy. When necessary, the experimental system was purged with dry nitrogen. Stress transients were measured with a piezoelectric detector [4,5] where the gelatin sample spontaneously adhered to the piezoelectric surface. A cw HeNe beam, parallel to the sample surface, was passed within 10 μm of the gelatin surface and monitored by a silicon photodiode. The samples were 13% wt/vol gelatin (Kroger Foods, Inc.) dissolved in deionized water (18 MΩ; $>60\,^{\circ}$C) and cast into films about 780 μm thick. Typically five measurements were performed on each sample, where the sample was translated to a fresh site for each exposure.

We have investigated the dynamics of gelatin ablation due to FEL irradiation at 3.0, 3.36, and 6.45 μm. 3.0 μm corresponds to the O–H stretch mode of water; 6.45 μm to the

*Present address: Physik Department E17, TU Munchen, D-85748 Garching, Germany.

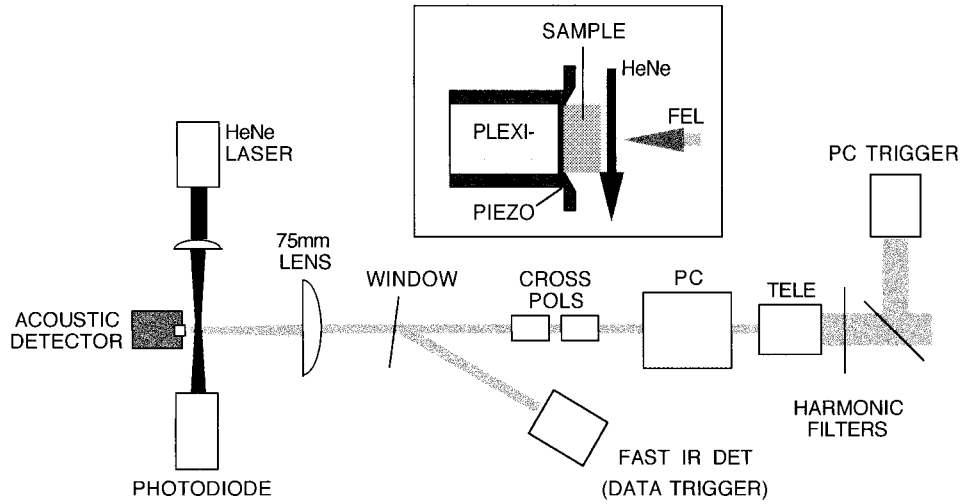

FIG. 1. Experimental design. The FEL beam enters from the right and harmonics are filtered out using antireflection coated silicon (6.45 μm) or germanium (3–4 μm). The telescope (TELE) reduction is either 20:3 (6.45 μm) or 15:3 (near 3 μm). Either a Brewsters cut or normal incidence Pockels cell (PC) was used. The fast infrared detector (FAST IR DET) is an electromagnetically coupled photodiode with 500 ps response time. The silicon photodiode that detects the HeNe ''shadow'' has a 25 ns response time. Details of the acoustic detector–sample compartment are shown in the inset. A 9 μm thick PVDF piezoelectric film (A.M.P. Corporation) was used. Electronic detection utilized a unity gain buffer with a 500 MHz bandwidth and a 10 ns cable delay, equivalent to that of the fast infrared detector and cable. Data was recorded using either an HP54522a digitizing oscilloscope with 500 MHz bandwidth and maximum sampling rate of 2 G samples/s or a Tektronix digitizer with 750 MHz bandwidth and a SRS235 delay generator.

amide II mode of gelatin and, to a lesser extent, overlaps the bending mode of water; 3.36 μm corresponds to the C–H stretch mode of gelatin and, to quite a substantial degree, the shoulder of the O–H stretch mode of water [1]. The absorption depth at 3.36 μm is approximately the same as that at 6.45 μm. Table I lists exposure parameters for each wavelength. A more detailed discussion of the experiment is available for the interested reader [5].

III. RESULTS

Typical stress transients generated by FEL fluences below the ablation threshold are displayed in Fig. 2. Exposures of 100 ns and 200 ns are presented, corresponding to approximately 300 and 600 micropulses, respectively. Each micropulse apparently generates a bipolar thermoelastic wave: the series of waves interfere according to Boltzmann's principle of superposition [6], yielding the detection of a compressive phase, a region of destructive interference, and a tensile phase. The observed compressive and tensile phases are approximately separated by τ, the ''macropulse'' duration as transmitted through the Pockels cell.

The influence of τ on tissue ablation due to 6.45 μm radiation is summarized in Fig. 3, where the micropulse fluences are above the ablation threshold and approximately constant for all τ's. The left column displays stress transients and the right column displays the simultaneously recorded shadow signal due to the interruption of the HeNe beam for τ's of 60 ns, 100 ns, and 200 ns. The stress transients reveal both the compressive and tensile phases of the thermoelastic wave, separated by τ as before, superposed with the contribution due to momentum recoil. The HeNe beam monitors the shadow cast on the silicon detector, demonstrating two minima (shadow maxima) of interest. One maximum of the shadow consistently occurs at approximately 1 μs [Figs. 3(a′)–3(c′)], followed by a more variable but routinely later second maximum. For longer τ's the initial maximum becomes obscured: this observation highlights the advantage of using a Pockels cell in this investigation.

TABLE I. Exposure Parameters. Note that the total fluence delivered in a 100 ns ''macropulse'' would be the tabulated value multiplied by 285.

Wavelength (μm)	Absorption depth (μm)	Spot radius (μm)	Fluence[a] (J/m^2)
3.0	<1	56	32–85
3.36	11	59	74–272
6.45	11	110	15–94

[a]The range of micropulse fluences are listed.

Figure 4 displays the stress transients and shadow signals for three wavelengths, where τ was uniformly 100 ns. At 3.0 μm the momentum recoil persists until about 300 ns, while at 6.45 μm and 3.36 μm the momentum recoil persists well past 300 ns. At 3.0 μm a single maximum shadow and a duration of approximately 5 μs were observed, while at 6.45 μm and 3.36 μm a second maximum was resolved and the ablation plume persists for approximately 15 μs.

The effect of micropulse fluence is summarized in Fig. 5, where fluences below the ablation threshold, just above the ablation threshold, and well above the ablation threshold at 3.36 μm are presented. All of the measured wavelengths exhibited the general pattern of a thermoelastic component for subablative and, at ablative fluences, an additional contribution due to momentum recoil whose integrated area increased with delivered energy. Figure 6 plots the peak momentum recoil as a function of micropulse fluence for 3.0 μm and 6.45 μm, where τ is uniformly 100 ns. The rise time

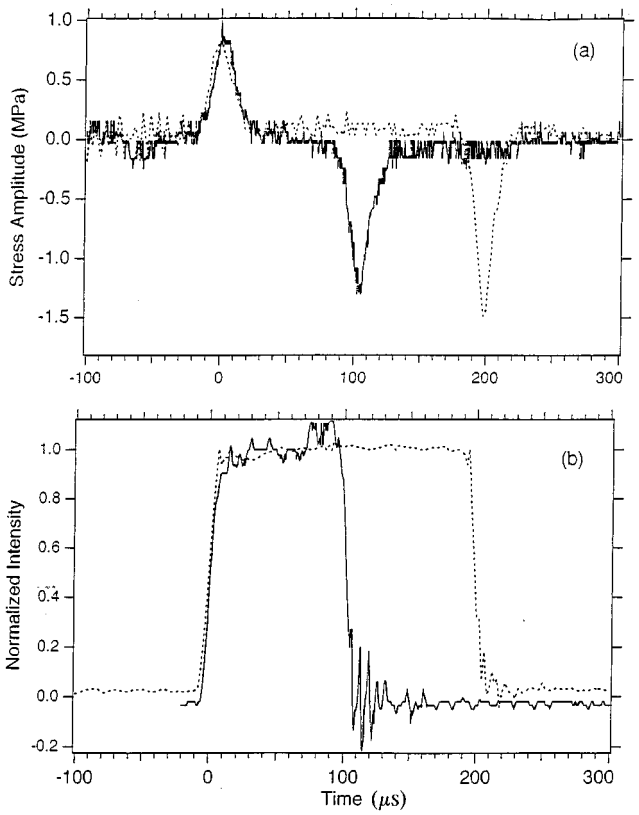

FIG. 2. Superposition of the thermoelastic response to FEL micropulses. (a) The acoustic stress transients measured after either 100 ns (0.15 mJ; solid line) or 200 ns (0.31 mJ; dashed line) subablative pulses at 6.45 μm. The separation between the positive (compressive) and negative (tensile) phases correlate with τ, the duration of the ''macropulse'' as transmitted by the Pockels cell. The experimental rise time of the thermoelastic wave ($\tau = 100$ ns) is 7.6 ns, based on an exponential fit, in good agreement with the theoretical value of 7 ns. (b) The corresponding optical pulse, demonstrating the envelope of FEL micropulses, as measured by the fast IR detector.

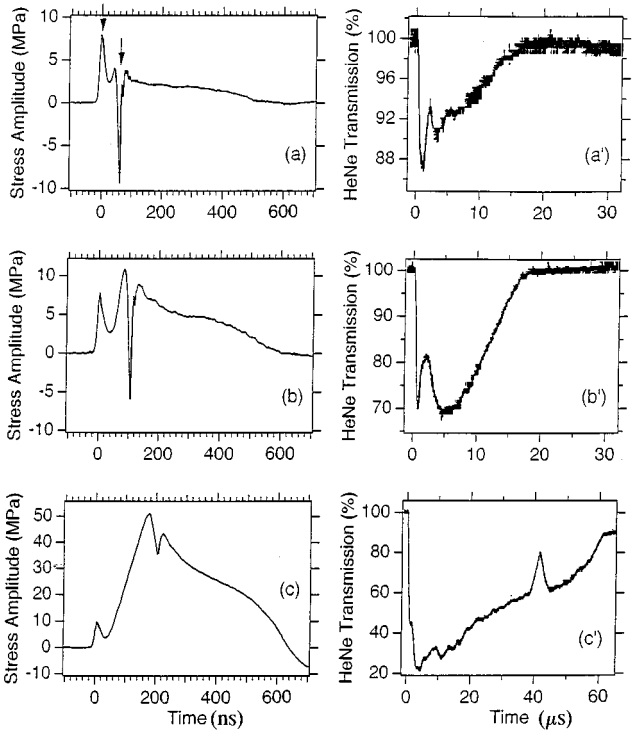

FIG. 3. Effect of macropulse duration (τ) on ablation dynamics. The FEL wavelength was 6.45 μm and fluence per *micropulse* was 94 J/m^2 throughout. The left column (a)–(c) displays measured stress transients. The right column (a′)–(c′) displays measurements of the ''shadow'' of the HeNe beam monitoring the onset of the ablation plume. Viewed horizontally, from top to bottom, are simultaneous measurements at total delivered energies of 0.7, 1.0, and 1.9 mJ with τ's of 60, 100, and 200 ns, respectively. In the acoustic data, note the compressive and tensile components of the thermoelastic contribution as indicated by arrows in (a), and evident in all three acoustic measurements. The magnitude of the compressive phases are approximately constant in (a)–(c): the tensile phases are similarly related, but with a larger magnitude than the compressive phases. In each of the shadow measurements (a′)–(c′), two principle local minima are resolved, corresponding to two maxima in the shadow. Note that the depth and duration of the second, later maximum scales with total delivered energy, correlating with the duration and magnitude of momentum recoil in the stress measurements. For shadow measurements, it is traditional to report the time required for the transmission to decrease by 10%: 280 ± 96 ns, 280 ± 33 ns, and 279 ± 27 ns for (a′), (b′), and (c′), respectively.

of the leading compressive phase is 5–8 ns at 3.36 and 6.45 μm, consistent with a thermoelastic mechanism. In addition, the magnitude of the compressive and tensile phases of the thermoelastic wave are proportional to the micropulse fluence, albeit with different constants of proportionality, as shown in Figs. 3 and 5. The electronics were not fast enough to resolve the onset of the compressive phase at 3.0 μm.

IV. DISCUSSION

Measurements of the stress transients uniformly demonstrate an essentially thermoelastic component, where the observed bipolar nature is consistent with a free surface and superposition of the micropulse-induced thermoelastic waves. The rise time of the leading compressive phase is consistent with a thermoelastic mechanism. However, there is an asymmetry between the observed compressive and tensile phases, evident both in amplitude and acoustic pulse shape. These observations are consistent with the evolution of material properties, e.g., absorption depth or the coefficient of thermal expansion, during exposure, as has been observed previously [7]. A more complete discussion of FEL-induced thermoelastic waves at subablative fluences will be published elsewhere [8].

HeNe monitoring of the ablation plume reveals a relatively fast process for all measured wavelengths that peaks at about 1 μs. Ablation at 3.0 μm is characterized by a single peak in the ablation plume. At 3.36 and 6.45 μm a second peak is also observed at a variable but always later time. As τ and/or the fluence increase, the 1 μs peak can become obscured by the increasing magnitude of the later process.

Figure 5 provides some insight into dynamics on the 10 ns time scale, demonstrating that the compressive phase of the thermoelastic component scales with micropulse fluence. In addition, the momentum recoil, the amount of plume, and the duration of ablation increase with micropulse fluence. Measurements of the peak recoil stress, summarized in Fig. 6,

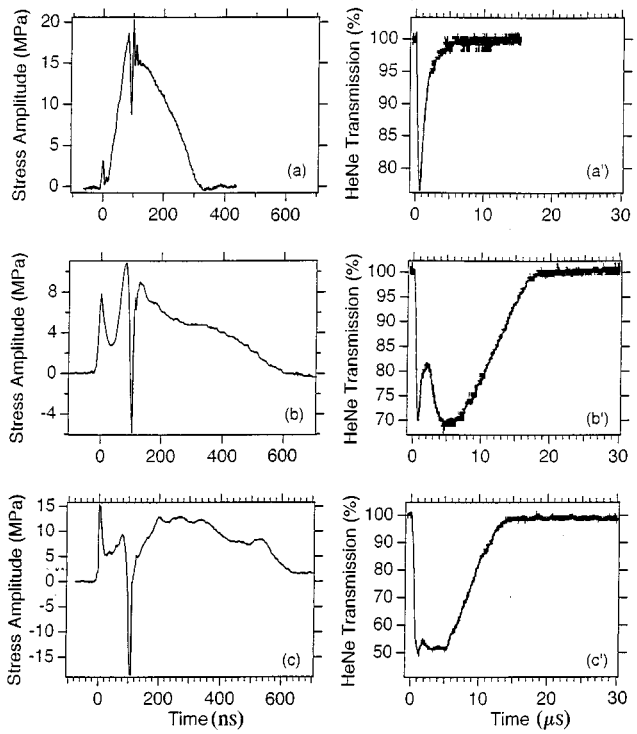

FIG. 4. Effect of infrared wavelength on ablation dynamics. The left column (a)–(c) displays measured stress transients. The right column (a′)–(c′) displays shadow measurements of the onset of the ablation plume. Viewed horizontally, from top to bottom, the exposure parameters were 3.0 μm (0.2 mJ ''macropulse'' energy; 71 J/m^2 micropulse fluence), 6.45 μm (1.0 mJ; 94 J/m^2), and 3.36 μm (0.48 mJ; 154 J/m^2).

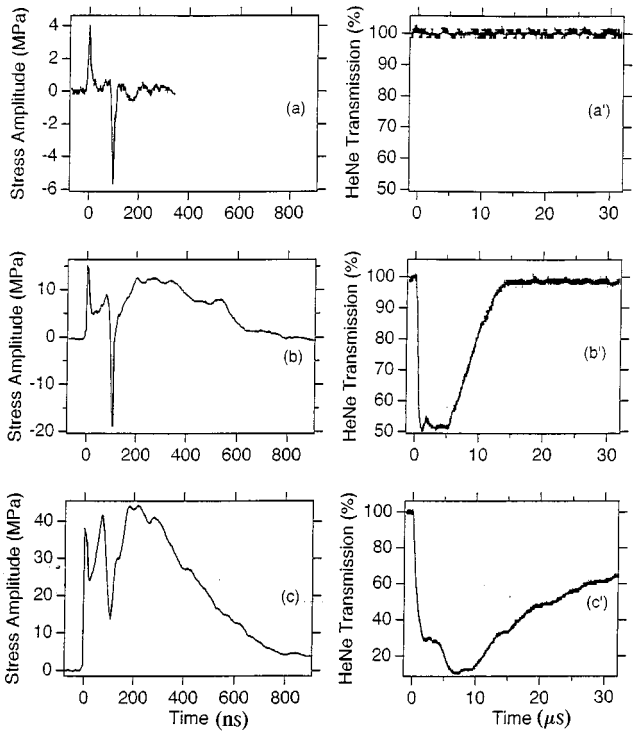

FIG. 5. Effect of micropulse fluence on ablation dynamics. The FEL wavelength was 3.36 μm and $\tau = 100$ ns throughout. The left column (a)–(c) displays measured stress transients. The right column (a′)–(c′) displays shadow measurements of the onset of the ablation plume. Viewed horizontally, from top to bottom, the micropulse fluences used were 74 J/m^2 (0.23 mJ ''macropulse'' energy), 154 J/m^2 (0.48 mJ), and 272 J/m^2 (0.85 mJ).

demonstrate that 3.0 μm ablation is more forceful than 6.45 μm ablation, indicating stiffer material, higher sound velocity, etc., for ablation at 3.0 μm.

Previously proposed models for infrared ablation are based on mechanisms that include thermal confinement and explosive vaporization [9], stress confinement and cavitation [10], mechanical motion of tissue at preablative fluences [11], and selective absorption by tissue components [1,12]. The micropulse-to-micropulse duration is about 350 ps, complicating efforts for time-resolved measurements aiming to conclusively identify the dynamical details of the mechanism governing infrared tissue ablation. However, at this time one cannot rule out the possibility that this closely spaced train of micropulses may play a key role for effective IR tissue ablation. In fact, spectroscopic measurements using the FEL are frequently obscured by ''thermal runaway''; the key to effective ablation seems to depend crucially on the transition from a dynamical to a thermodynamic process. Furthermore, these experimental results, more specifically the asymmetry of the thermoelastic wave and the wavelength dependence for both the ablation plume and the ablative stress transients, indicate that the material properties of gelatin evolve during the 100 ns time regime and that the tensile strength of gelatin can be compromised during time scales that influence the ablation process, consistent with the partitioning of energy model that was based on thermodynamic reasoning [1]. The evidence for a photothermomechanical mechanism, with time-dependent mechanical properties, is mounting. Such a

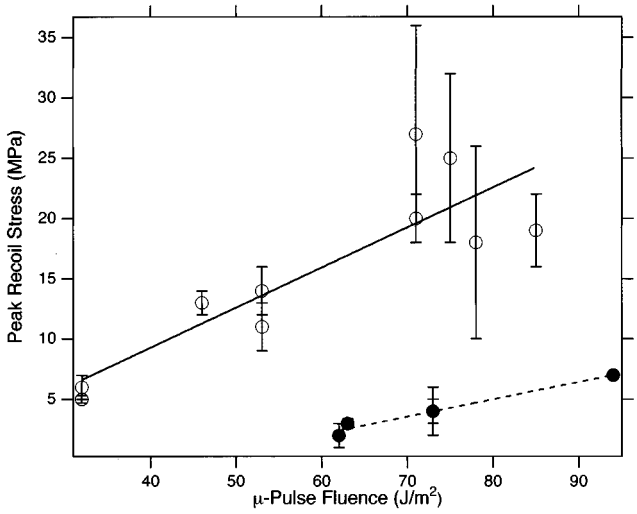

FIG. 6. Momentum Recoil as a function of fluence at 3.0 μm (open circles) and 6.45 μm (solid circles). The peak of the momentum recoil in the stress transient is plotted vs the micropulse fluence. Each data point represents at least five single shot recordings. The error bars represent one standard deviation. The best-fit lines have slopes of 0.14 and 0.33 MPa m^2/J for 6.45 and 3.0 μm, respectively.

mechanism builds upon and unifies several of the previous models for infrared tissue ablation.

There are several key experimental findings that will need to be addressed by any model that accounts for infrared ablation of tissue. The shadow measurements reported here indicate one resolved process for 3.0 μm and two processes at 3.36 and 6.45 μm, while the measurements of stress transients demonstrate that the duration of the momentum recoil is significantly longer at 3.36 and 6.45 μm relative to 3.0 μm. More generally, while mechanical effects suggest a qualitative explanation for the discrepancy associated with models solely based on vaporization, a quantitative dynamical model that includes mechanical effects has yet to gain acceptance. Furthermore, while mechanical models address the preablative evolution of mechanical stress, a comprehensive dynamical model that crosses from the subablative to the ablative regime is not available.

Gelatin is a disordered, entangled polymer system; in contrast, collagen is a highly ordered system with substantially greater tensile strength [13]. Caution should be used in generalizing these results to collagenous tissue. In the future we plan to extend these measurements to corneal stroma, a resilient and highly ordered collagenous material, and other tissues. In addition, we plan to improve on our past experiments using two parallel HeNe beams to monitor the plume [5] with the goal of determining the velocity distribution of ablated particles.

Lasers are a standard tool for a number of medical applications [14], including retinal surgery with visible lasers, where the mechanism for tissue modification is photocoagulation [15], and corneal surgery with ultraviolet lasers [16] based on the basic research of Srinivasan [17]. There are some limitations, however, associated with the complications of photochemistry due to visible and especially ultraviolet photons. Consequently, in the past biomedical investigators have also explored the potential of infrared lasers. Previous investigations of ablation with CO_2 as well as Nd: yttrium aluminum garnet (YAG) and Er:YAG lasers demonstrate moderate thermal and/or mechanical damage to collateral tissue [14]. While thermal damage serves a useful hemostatic purpose for many medical applications, this amount of collateral damage can be prohibitive, especially for cornea and neural tissues. Ablation with wavelengths near 6.45 μm have the potential to overcome some of the limitations of conventional lasers. Surgical applications of the Mark-III FEL currently are under investigation at the Vanderbilt FEL Center [18].

V. CONCLUDING REMARKS

The key finding of this investigation is the observation of a sole early process for ablation at 3.0 μm and an additional, slower process at 3.36 and 6.45 μm. In addition, we can account for the subablative stress transients in terms of superposed, asymmetric thermoelastic waves, while ablative stress transients are accounted for in terms of the superposition of an asymmetric thermoelastic wave with momentum recoil. The durations of both the plume and the momentum recoil indicate that ablated material is stiffer for 3.0 μm ablation than it is for ablation at 3.36 or 6.45 μm. These results challenge current models of infrared tissue ablation.

ACKNOWLEDGMENTS

This work was supported by the DoD MFEL program under Contract No. N00014-94-1-1023. We thank Apostolos Doukas for insightful comments.

[1] G. Edwards *et al.*, Nature **371**, 416 (1994).
[2] C. A. Brau, Nucl. Instrum. Methods Phys. Res. A **319**, 47 (1992).
[3] K. Becker, J. B. Johnson, and G. Edwards, Rev. Sci. Instrum. **65**, 1496 (1994).
[4] M. Sigrist, Appl. Phys. **60**, R83 (1986).
[5] J. Tribble, Ph.D. thesis, Vanderbilt University, 1996.
[6] H. Kolsky, *Stress Waves in Solids* (Clarendon, Oxford, 1963), p. 112.
[7] K. L. Vodopyanov, J. Chem. Phys. **94(8)**, 5389 (1991); J. P. Cummings and J. T. Walsh, Appl. Phys. Lett. **62**, 1988 (1993); J. T. Walsh and J. P. Cummings, Lasers Surg. Med. **15**, 295 (1994).
[8] J. Tribble and G. Edwards (unpublished).
[9] M. L. Wolbarsht, IEEE J. Quantum Electron. **QE-20**, 1427 (1984); J. T. Walsh, T. J. Flotte, and R. R. Anderson, Lasers Surg. Med. **8**, 108 (1988); V. Venugopalan, N. S. Nishioka, and B. B. Mikic, Biophys. J. **70**, 2981 (1996).
[10] R. S. Dingus and R. J. Scammon, Laser Tissue Interactions II (SPIE) **1427**, 45 (1991); G. Paltauf and H. Schmidt-Kloiber, Lasers Surg. Med. **16**, 277 (1995).
[11] I. Itzkan *et al.*, Proc. Natl. Acad. Sci. USA **92**, 1960 (1995).
[12] R. R. Anderson and J. A. Parrish, Science **220**, 524 (1983).
[13] P. J. Flory, *Statistical Mechanics of Chain Molecules* (Hanser, New York, 1969), Chap. 7.
[14] *Lasers in Biology and Medicine*, edited by R. R. Alfano and A. G. Doukes, special issue of IEEE J. Quantum Electron. **QE-20**, 1342 (1984); *New Developments in Opthalmic Lasers*, edited by C. A. Puliafito, special issue of Lasers Surg. Med. **15**, 126 (1994); S. Krisnamurthey and S. K. Powers, *ibid.* **15**, 126 (1994); R. H. Ossoff *et al.*, *ibid.* **15**, 217 (1994); L. I. Deckelbaum, *ibid.* **15**, 315 (1994); H. A. Wigdor *et al.*, *ibid.* **16**, 103 (1995); M. Krauss and C. A. Puliafito, *ibid.* **17**, 102 (1995); R. Reid and G. T. Absten, *ibid.* **17**, 201 (1995).
[15] C. J. Koester *et al.*, J. Opt. Soc. Am. **52**, 607 (1962).
[16] S. Trokel, J. Cataract Refractive Surg. **15**, 373 (1989).
[17] R. Srinivasan, Science **234**, 559 (1986).
[18] G. Edwards *et al.*, J. Spec. Top. Quantum Electron. **2**, 810 (1996).